Progress In Electromagnetics Research, PIER 12, 1–35, 1996

MINIMIZATION OF THE COUPLING BETWEEN A TWO CONDUCTOR MICROSTRIP TRANSMISSION LINE USING FINITE DIFFERENCE METHOD

A. Z. Elsherbeni, C. E. Smith, and B. Moumneh

1. Introduction

Microstrip coupled transmission lines have been studied extensively for applications as couplers and filters [1] and even applications as sensors using a wide variety of analysis methods [2]. However, in some applications, it is necessary to modify the basic geometry of the microstrip lines to reduce or eliminate undesirable properties such as spurious capacitive and coupling effects [1,3]. As computer clock rates and frequency of operation increase and interline spacings decrease, the need for accurate analysis of the coupling between multi-layered microstrip transmission lines becomes very important. The distortion due to the differences in even and odd mode propagation must also be carefully studied and controlled. Furthermore, in order to achieve signal transmission without any interference, the coupling between adjacent lines should be minimized. The effect of capacitive coupling on

the properties of microstrip transmission lines is of increasing importance because of high-power applications and emphasis on size reduction and packaging. Examples are found in monolithic microwave integrated circuits (MMIC). This technology began in the late 50s with circuits etched on copper plated plastic sheets. It has now evolved to a point where industrial MMICs are batch processed on substrates (silicon or gallium arsenide) which includes interconnecting transmission lines and semiconductor elements (diodes and transistors). Package dimensions are kept small as in analogue and digital ICs, and MIC circuit elements and interconnections are densely packaged to obtain circuit miniaturization. The effects of these closely spaced circuit elements, interconnections, sidewalls, and package covers are similar to those of digital and analogue ICs and can greatly influence the behavior of high speed, high density integrated circuits and modules. Thus, the coupling or crosstalk effects on MMICs are also of great interest to the MMIC design engineer.

Over the past few decades, microstrip transmission lines (MTLs) have been analyzed extensively to develop accurate and fast techniques for design and fabrication of high frequency circuits. The method of moments has been a primary candidate for solving transmission line problems [4-7]. Some other techniques have also been used to solve these problems. To cite only a few of those studies, Yamashita analyzed a single-strip shielded transmission line using the variational method technique [8]. Gladwell studied the behavior of the shielded and unshielded coupled microstrip problem where the charge distribution on the strips was expanded using Chebyshev polynomials [9]. Cohn presented rigorous formulas for the odd and even characteristic impedance of single and coupled microstrip lines [10]. Methods for computing the line capacitance of transmission line using dual and triple integral equations have been investigated [11]. The theory of quasi-TEM modes on coupled transmission lines in terms of voltage and current eigenvectors was developed by Kajfez [12]. He has shown that the even and odd propagating modes are possible only when the coupled transmission line is of symmetric shape. The purpose of this research is to present a finite difference (FD) solution to analyze and further control the coupling between the lines. This study introduces the possibility of having a MTL embedded in or above a ground plane as shown in Figs. 1 and 2. The analysis starts with the use of Lagrangian polynomials which have been used to approximate the second order differential

equation in Laplace's equation. Then, the integral form of Gauss's law is used to derive an expression for the scalar potential on the dielectric interfaces. An approximate (asymptotic) boundary condition (ABC) at the artificial boundary is used to truncate the nonuniform FD mesh. This method can handle finite and infinitely thin strips, however, we did not include the strips thickness in our analysis in order to minimize the complexity of the transmission line geometry. The charges on the strips are computed from the potential distribution, then the MTL parameters are evaluated. Finally, methods for controlling both coupling capacitance and phase velocities of the even and odd modes are discussed through numerical examples of open and embedded coupled MTLs. These results will aid the microwave engineer in the design and fabrication of microwave and millimeter wave MMICs as well as provide a basis for continued development of computer-aided-design and simulation of these type circuits.

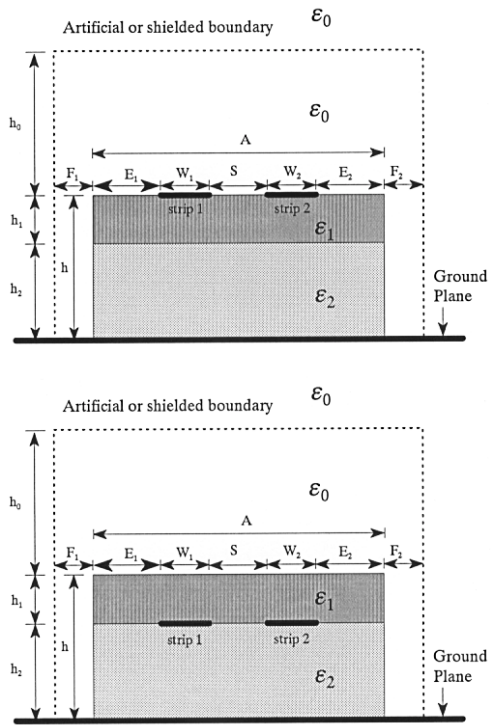

Figure 1. Geometries of microstrip transmission lines above a ground plane.

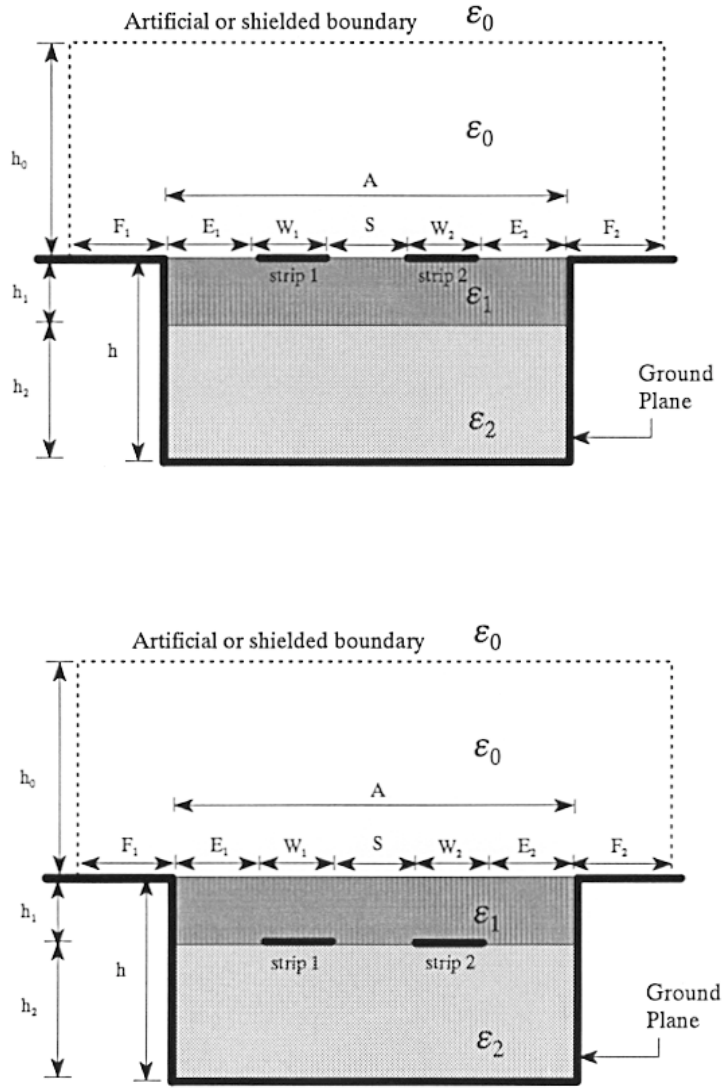

Figure 2. Geometries of microstrip transmission lines embedded in a ground plane.

2. Finite Difference Analysis

For the quasi-static 2D problems shown in Figs. 1 and 2, the potential V can be described using Laplace's equation by:

$$\frac{\partial^2 V}{\partial x^2} + \frac{\partial^2 V}{\partial y^2} = 0 \tag{1}$$

The FD technique approximates the derivatives involved in Laplace's equation based on the potential at a certain node in terms of the potential at neighboring grid points, or nodes. In general, assuming that we have three consecutive nodes $L, P, R,$ as shown in Fig. 3, Lagrange's form of interpolating polynomial is described as [13]

$$\begin{aligned} f(x) \simeq P_2(x) = & \frac{(x-x_P)(x-x_R)}{(x_L-x_P)(x_L-x_R)} f(x_L) \\ & + \frac{(x-x_L)(x-x_R)}{(x_P-x_L)(x_P-x_R)} f(x_P) \\ & + \frac{(x-x_L)(x-x_P)}{(x_R-x_L)(x_R-x_P)} f(x_R) \end{aligned} \tag{2}$$

where $P_2(x)$ represent a second degree polynomial which coincides with the exact values of the function $f(x)$ at the three nodes L, P, R. In order to apply Laplace's equation over the potential $V(x, y)$, the second order derivatives need to be approximated in both the x and y directions. The Lagrange interpolating polynomial will then have to be differentiated twice. That is,

$$\begin{aligned} \frac{df(x)}{dx} = & \frac{(x-x_P)+(x-x_R)}{(x_L-x_P)(x_L-x_R)} f(x_L) + \frac{(x-x_L)+(x-x_R)}{(x_P-x_L)(x_P-x_R)} f(x_P) \\ & + \frac{(x-x_L)+(x-x_P)}{(x_R-x_L)(x_R-x_P)} f(x_R) \end{aligned} \tag{3}$$

$$\begin{aligned} \frac{d^2 f(x)}{dx^2} = & \frac{2f(x_L)}{(x_L-x_P)(x_L-x_R)} + \frac{2f(x_P)}{(x_P-x_L)(x_P-x_r)} \\ & + \frac{2f(x_R)}{(x_R-x_L)(x_R-x_P)} \end{aligned} \tag{4}$$

Similar expressions for the derivatives with respect to the y coordinate can be obtained.

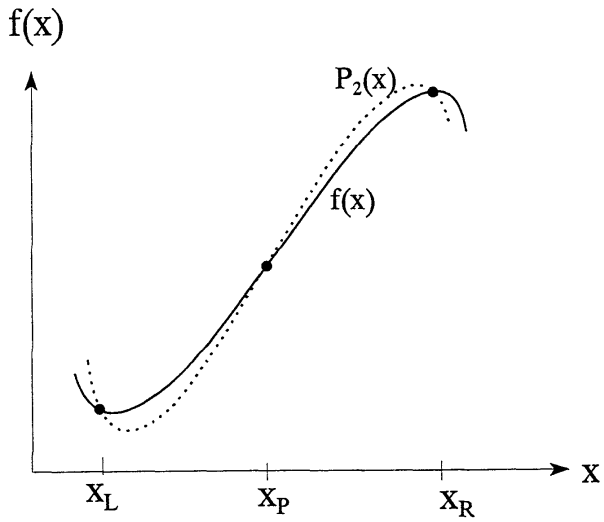

Figure 3. Second degree Lagrangian interpolating function.

The boundary conditions for the MTLs shown in Figs. 1 and 2 are: $V = V^1$ on strip 1; $V = V^2$ on strip 2; $V = 0$ on the ground plane; and at a point on a dielectric interface $\oint_s \vec{D} \cdot \vec{ds} = Q$, where Q is the charge on the dielectric interfaces surrounded by the closed surface s. Applying Laplace's equation to point C in a homogeneous source free region yields

$$\begin{aligned} &\frac{V_L}{(x_L - x_C)(x_L - x_R)} + \frac{V_C}{(x_C - x_L)(x_C - x_R)} \\ &\quad + \frac{V_R}{(x_R - x_L)(x_R - x_C)} + \frac{V_T}{(y_T - y_C)(y_T - y_B)} \\ &\quad + \frac{V_C}{(y_C - y_T)(y_C - y_B)} + \frac{V_B}{(y_B - y_C)(y_B - y_T)} = 0 \end{aligned} \tag{5}$$

where the subscripts $L, R, B,$ and T refer to the left, right, bottom and top nodes relative to node C. It is important to note that this type of analysis applies to uniform as well as to nonuniform meshes. At the intersection between four different homogeneous dielectric source

free regions as shown in Fig. 4, Gauss's law is applied over a closed surface surrounding C which yields

$$\begin{aligned}\frac{-V_C}{2}\Big[\frac{\varepsilon_1+\varepsilon_2}{y_T-y_C}+\frac{\varepsilon_1+\varepsilon_4}{x_C-x_L}+\frac{\varepsilon_4+\varepsilon_3}{y_C-y_B}+\frac{\varepsilon_3+\varepsilon_2}{x_R-x_C}\Big]\\ +\frac{V_T}{2}\left(\frac{\varepsilon_1+\varepsilon_2}{y_T-y_C}\right)+\frac{V_L}{2}\left(\frac{\varepsilon_1+\varepsilon_4}{x_C-x_L}\right)\\ +\frac{V_B}{2}\left(\frac{\varepsilon_4+\varepsilon_3}{y_C-y_B}\right)+\frac{V_R}{2}\left(\frac{\varepsilon_3+\varepsilon_2}{x_R-x_C}\right)=0\end{aligned} \tag{6}$$

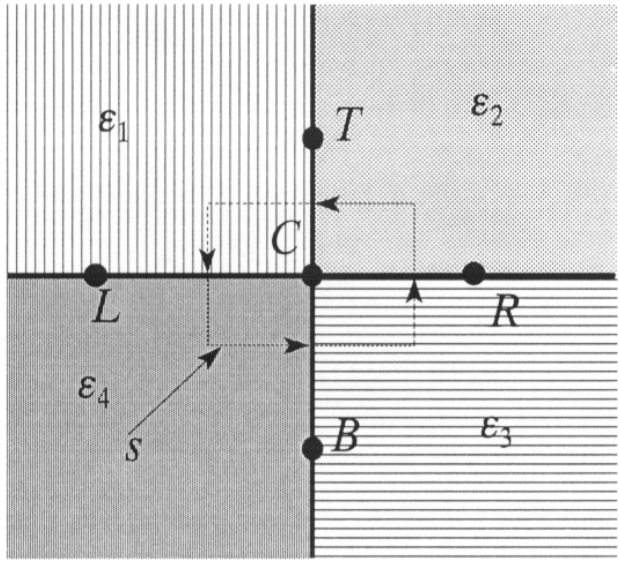

Figure 4. Node C between 4 different homogeneous dielectric media.

The main advantage of the FD technique is that the resulting matrix is banded and can be easily manipulated using well known matrix inversion routines. Contrary to the finite element method, the construction of a sparse or banded matrix requires much more involved node arrangements.

3. Approximate Boundary Condition

For the MTLs shown in Figs. 1 and 2, the outer artificial boundary could be grounded perfect conductor (shielded), and hence, the potential at the boundary is set to zero. However, when the transmission line is not shielded by a ground plane, an approximate boundary condition (ABC) should be applied at that boundary in order to truncate the infinite mesh so that numerical analysis could be carried out. The ABC used here is proposed by Khebir, et. al. [14], and used by Gordon and Fook for a simpler geometry [15]. Therefore, only the final expressions needed are listed here. The finite difference approximation for a point C on the right boundary as shown in Fig. 5 is given by

$$\begin{aligned} &V_L[K_R + K_L] + V_C[K_R C_C + K_P] \\ &\quad + V_B[K_R C_B + K_B] + V_T[K_R C_T + K_T] = 0 \end{aligned} \tag{7}$$

where

$$\begin{aligned} C_C &= \frac{-2\Delta}{x_C}\left(1 + y_C \frac{(y_C - y_B) + (y_C - y_T)}{(y_C - y_B)(y_C - y_T)}\right) \\ C_B &= \frac{-2\Delta y_C}{x_C}\left(\frac{(y_C - y_T)}{(y_B - y_C)(y_B - y_T)}\right) \\ C_T &= \frac{-2\Delta y_C}{x_C}\left(\frac{(y_C - y_B)}{(y_T - y_B)(y_T - y_C)}\right) \end{aligned} \tag{8}$$

$$\begin{aligned} K_L &= \frac{1}{(x_L - x_C)(x_L - x_R)}, \quad K_R = \frac{1}{(x_R - x_L)(x_R - x_C)} \\ K_T &= \frac{1}{(y_T - y_C)(y_T - y_B)}, \quad K_B = \frac{1}{(y_B - y_C)(y_B - y_T)} \\ K_C &= \frac{1}{(x_C - x_L)(x_C - x_R)} + \frac{1}{(y_C - y_T)(y_C - y_B)} \end{aligned} \tag{9}$$

On the left boundary the corresponding expression is

$$\begin{aligned} &V_R[K_L + K_R] + V_C[-K_L C_C + K_C] \\ &\quad + V_B[-K_L C_B + K_B] + V_T[-K_L C_T + K_T] = 0 \end{aligned} \tag{10}$$

and for the top side of the outer boundary, we obtain

$$V_B[K_T+K_B]+V_C[K_TC'_C+K_C]+V_R[K_TC'_R+K_R]+V_L[K_TC'_L+K_L]=0 \tag{11}$$

where

$$\begin{aligned} C'_C &= \frac{-2\Delta}{y_C}\left(1+x_C\frac{(x_C-x_L)+(x_C-x_R)}{(x_C-x_L)(x_C-x_R)}\right) \\ C'_R &= \frac{-2\Delta x_C}{y_C}\left(\frac{(x_C-x_L)}{(x_R-x_L)(x_R-x_C)}\right) \\ C'_L &= \frac{-2\Delta x_C}{y_C}\left(\frac{(x_C-x_R)}{(x_L-x_C)(x_L-x_R)}\right) \end{aligned} \tag{12}$$

At the right corner of the artificial boundary, we get

$$V_C\rho_C+V_B\left(-\rho_B+\rho_B\frac{\phi_C-\phi_B}{\phi_L-\phi_B}\right)+V_L\left(-\rho_L\frac{\phi_C-\phi_B}{\phi_L-\phi_B}\right)=0 \tag{13}$$

And at the left corner, we obtain

$$V_C\rho_C+V_R\left(-\rho_R+\rho_B\frac{\phi_C-\phi_R}{\phi_B-\phi_R}\right)+V_B\left(-\rho_B\frac{\phi_C-\phi_R}{\phi_B-\phi_R}\right)=0 \tag{14}$$

where the angles are defined in Fig. 5.

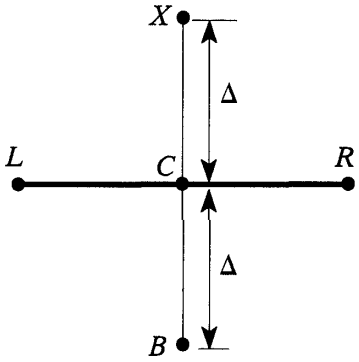

(a) Top boundary

Figure 5. Setup system for ABC.

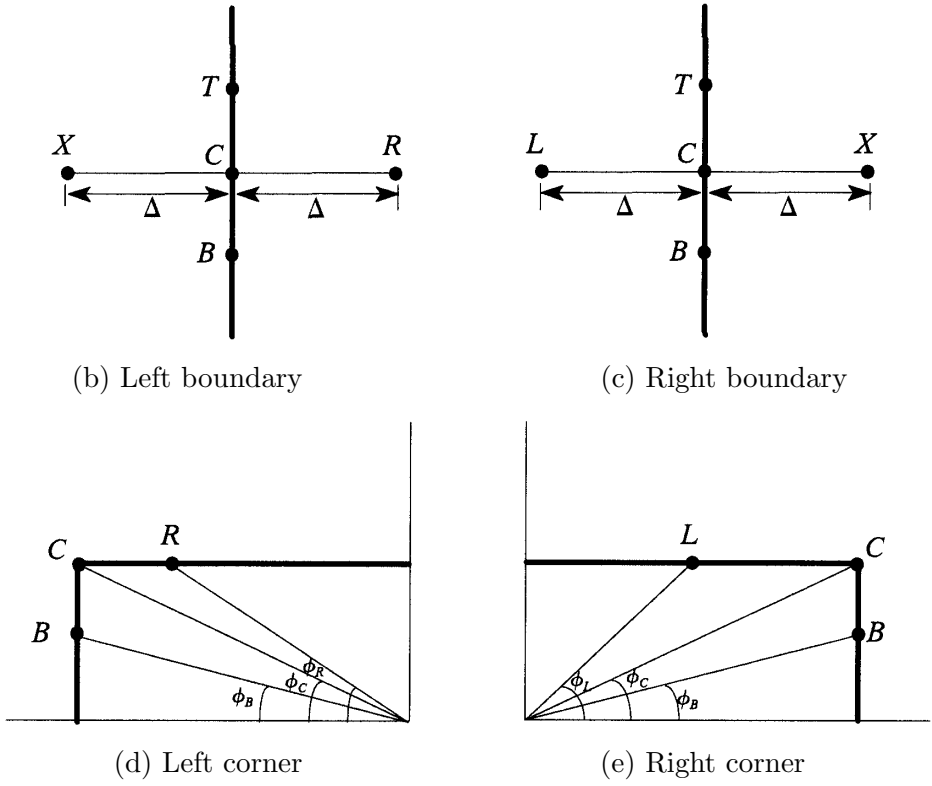

(b) Left boundary (c) Right boundary

(d) Left corner (e) Right corner

Figure 5. Setup system for ABC.

4. Computation of Total Charge and Line Parameters

To find the characteristic impedance and the phase velocities for a transmission line having an inhomogeneous medium requires calculating the capacitances of the structure, with and without the dielectric substrate [16]. Since the capacitance per unit length is directly related to the charge per unit length on the strips, the problem is reduced to finding the total charge per unit length on the strips. If Guass's law is applied to a closed path g enclosing the cross-section of the i^{th} conductor, the total charge per unit length on that conductor Q^i is then

expressed as:

$$Q^i = -\oint_g \varepsilon(x,y)\frac{\partial V(x,y)}{\partial n}dg \tag{15}$$

where n is a unit vector normal to the closed path g. The integral in equation (23) is converted to a numerical summation over the grid points surrounding the i^{th} strip [17]. In this process, the expression in equation (3) is used for the derivative of the potential. The self and coupling capacitances are then computed from the known total charge density on the strips using the following set of equations.

$$Q^1_{e,o} = C_{11}V^1_{e,o} + C_{12}(V^1_{e,o} - V^2_{e,o}) \tag{16}$$

$$Q^2_{e,o} = C_{21}(V^2_{e,o} - V^1_{e,o}) + C_{22}V^2_{e,o} \tag{17}$$

where the subscripts e and o represent the even and odd modes of propagation, respectively, and $V^1_e = V^1_o = V^2_e = -V^2_o = 1$. The expressions for the odd and even phase velocities (V_o, V_e) and characteristic impedances (Z_o, Z_e) in terms of the charges can then be written as

$$\nu_e = C\sqrt{\frac{Q_{ae}}{Q_e}}, \qquad \nu_o = C\sqrt{\frac{Q_{ao}}{Q_o}} \tag{18}$$

$$Z_{oe} = \frac{1}{C\sqrt{Q_eQ_{ae}}}, \qquad Z_{oo} = \frac{1}{C\sqrt{Q_oQ_{ao}}} \tag{19}$$

where C is the velocity of light and the subscript a stands for the charges with all dielectric materials replaced by air. When this coupled transmission line is used as a coupling device, its characteristic impedance is usually given by

$$Z_o = \sqrt{Z_{oe}\ Z_{oo}} \tag{20}$$

Another important parameter that describes the electrical coupling factor between strip 1 and strip 2 is defined as $k_e = \frac{V^2}{V^1}$, where V^2 is the voltage induced on strip 2 due to V^1 applied on strip 1 [18]. Hence, from the open circuit capacitive voltage splitting for a symmetric MTL, k_e for symmetric geometries reduces to

$$k_e = 20\ \log_{10}\left[\frac{C_{12}}{C_{11} + C_{12}}\right] \tag{21}$$

5. Numerical Results

Two separate programs have been written for the analysis of the MTLs shown in Figs. 1 and 2. In the following sections, all the numerical results shown here will be derived assuming that both conductors have the same number of grid points, that is NW1=NW2, unless otherwise specified. The code written for the MTL shown in Fig. 1 was tested and compared with results based on the method of moments [19]. The geometry selected was $W_1 = W_2 = 0.5$, $S = 0.5$, $E_1 = E_2 = 0.5$, $h_1 = h_2 = 0.5$, $h_0 = 1$, $F_1 = F_2 = 0.5$, $\varepsilon_{r1} = 9.7$, $\varepsilon_{r2} = 2.2$. Table 1 lists the values of Z_{oe}, Z_{oo}, C_{11}, and C_{12} along with the order of the matrix and the number of points on one strip for the two different solutions. As shown in Table 1, the results obtained from this study by using the FD technique along with the ABC and those from [19] agree very well. The advantage of using the FD technique over the MoM is that the matrix formed in the former is sparse and banded which, when taken advantage of, significantly reduces the CPU running time and the storage capacity. The CPU time is reduced by a factor of at least 100 when using banded matrix solver relative to a full matrix solver [20].

Technique	Z_{oe}	Z_{oo}	C_{11}	C_{12}	Matrix order	NW1
MoM	121.87	54.61	46.72	41.01	450	42
FD	123.17	53.09	46.36	42.84	2911	11

Table 1. Comparison between the computed MTL parameters using the MoM and FD solutions.

Another test was also performed to verify the developed code for the MTL shown in Fig. 2. A shielded MTL was selected such that $W_1 = W_2 = 0.5$, $S = 0.5$, $E_1 = E_2 = 3.25$, $h_1 = h_2 = 0.5$, $h_0 = 1$, $F_1 = F_2 = 0$, $\varepsilon_{r1} = \varepsilon_{r2} = 3.8$. The results obtained were then compared to the work done by Pompei, et. al., where the approach of their analysis may be summarized as an extension of Kirchhoff's theory to a system of N parallel coupled transmission lines [21]. The values of Z_{oe} and Z_{oo} have been graphically measured from Fig. 15 in [21] which are approximately 105.0 and 68.0, respectively, and our corresponding values are 103.42 and 66.89, respectively. Our values of Z_{oe} and Z_{oo} are in good agreement with those from [21] with a maximum difference of 1.5%.

The importance of placing the artificial boundary at the correct position is vital to the analysis of the MTL. It is always desired to place the artificial boundary as close to the strips as possible and yet not effect the performance of the line. The closer the distance from the artificial boundary to the strips, the smaller the mesh would be and, consequentially, less computer storage is required and faster execution is possible. In order to study the behavior of the MTL as the height and width of the artificial boundary changes, a geometry, similar to the one used for Table 1, was selected with the strips on top of the two substrates (strips up). The outer widths of the artificial boundary, F_1 and F_2, shown in Fig. 1, were then varied from 0.1 to 1.9 with $F_1 = F_2$ and $h_0 = F_1 + 0.5$. The results shown in Fig. 6 (strips up) suggest that the height of the artificial boundary should be of the order of the combined height of the substrates. The same geometry was then repeated with the strips in between the two substrates (strips down). It was found in this case that the artificial boundary could be placed at closer distances to the strips than with the strips up without a significant change in the behavior of the MTL, as shown in Fig. 6 (strips down). This kind of behavior for the transmission line is due to the fact that the field lines are heavily concentrated in the upper substrate. This concentration, however, depends on the dielectric constant of the upper substrate, the width of the strips, and their separation distance. Thus, having a relatively close artificial boundary, with the strips between the two substrates, does not significantly affect the performance of the transmission line. The same behavior is observed for the embedded microstrip line [20].

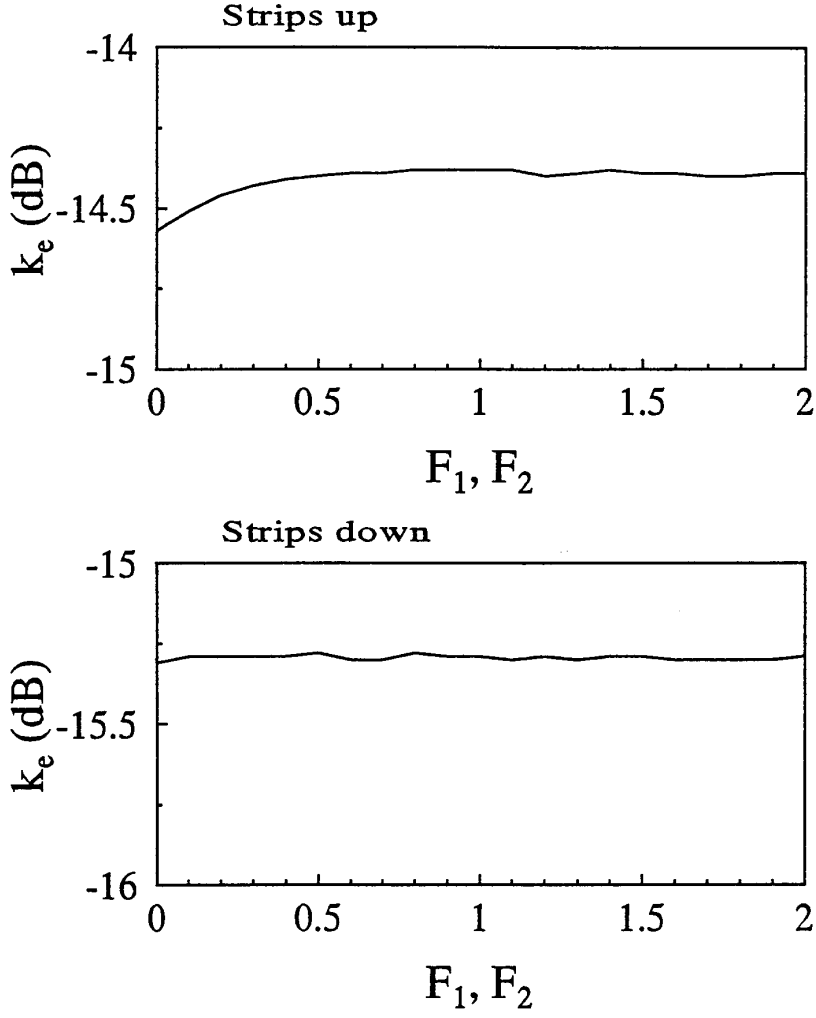

Figure 6. Coupling coefficient vs F_1, F_2 ($W_1 = W_2 = 0.5$, $S = 0.5$, $E_1 = E_2 = 0.5$, $h_1 = h_2 = 0.5$, $h_0 = F_1 + 0.5$, $A = 2.5$, $\varepsilon_{r1} = 9.7$, $\varepsilon_{r2} = 2.2$, $NW1 = 7$).

The convergence behavior of both even and odd mode characteristic impedances, Z_{oe} and Z_{oo}, is investigated, as the order of the matrix N is increased. Figure 7 shows Z_{oe} and Z_{oo} as a function of 1/N for the MTL geometry in Fig. 1. From this figure, one notices that the percentage error is less than 2% when the order of the matrix is 2000.

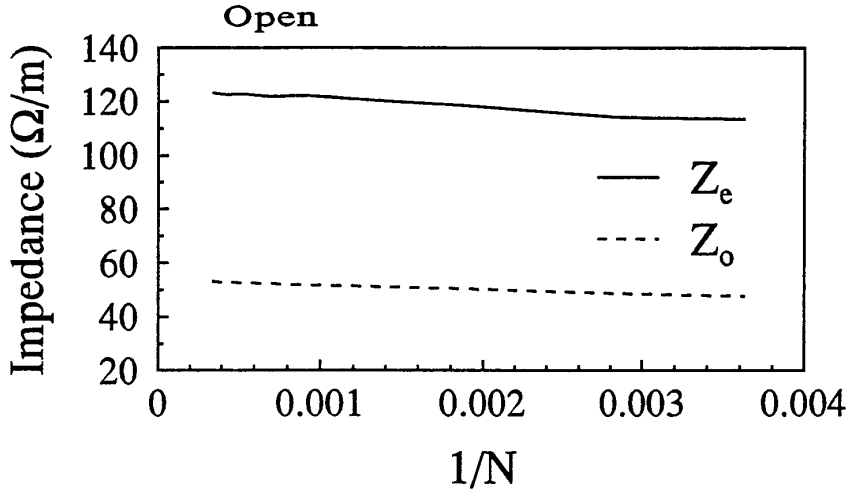

Figure 7. Convergence of impedance ($W_1 = W_2 = 0.5$, $S = 0.5$, $E_1 = E_2 = 0.5$, $A = 2.5$, $h_1 = h_2 = 0.5$, $h_0 = 1$, $F_1 = F_2 = 0.5$, $\varepsilon_{r1} = 9.7$, $\varepsilon_{r2} = 2.2$, strips up).

For the geometry shown in Fig. 2, the 3D plots of the potential distribution with shielded as well as ABC, are shown in Figs. 8 and 9, respectively. It is worth noting that the two conductors were raised to a potential of 1 volt each. The 3-D plots of the potential show that the potential on the artificial boundary takes a finite value, as expected, and drops to zero for the shielded case.

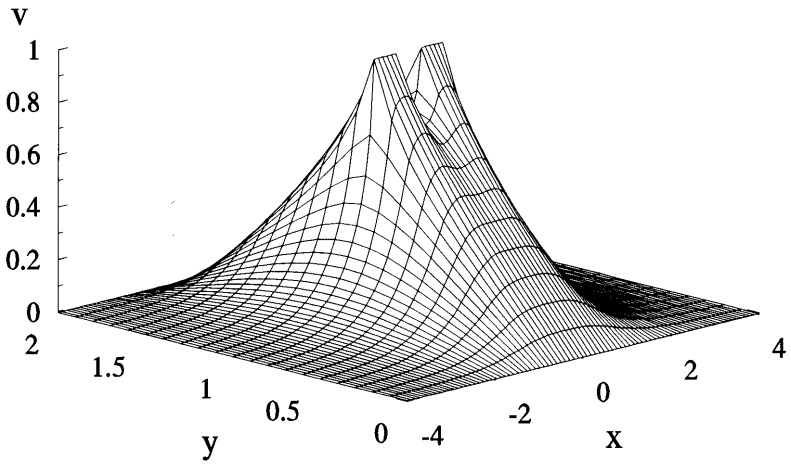

Figure 8. Potential distribution for shielded case ($W_1 = W_2 = 0.5$, $S = 0.5$, $E_1 = E_2 = 3.25$, $A = 8$, $h_1 = h_2 = 0.5$, $h_0 = 1$, $F_1 = F_2 = 0$, $\varepsilon_{r1} = \varepsilon_{r2} = 3.8$, $NW1 = 6$, strips up).

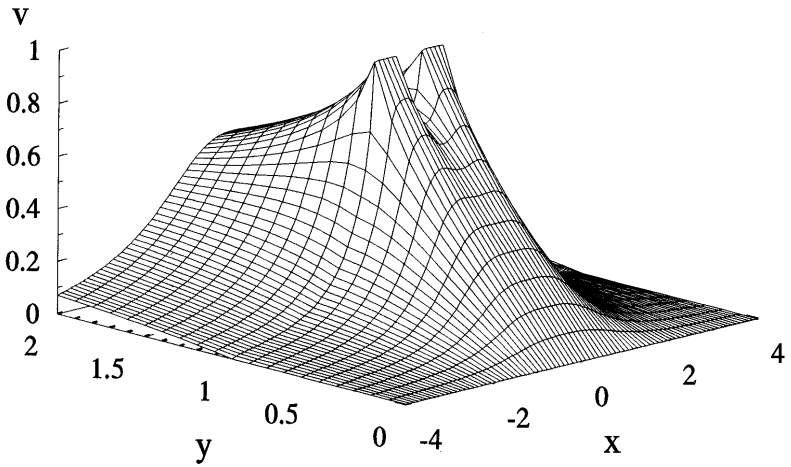

Figure 9. Potential distribution for ABC-1 ($W_1 = W_2 = 0.5$, $S = 0.5$, $E_1 = E_2 = 3.25$, $A = 8$, $h_1 = h_2 = 0.5$, $h_0 = 1$, $F_1 = F_2 = 0$, $\varepsilon_{r1} = \varepsilon_{r2} = 3.8, NW1 = 6$, strips up).

The effect of the dielectric constant of the substrate material was then studied. The geometry in Fig. 2, (embedded structure), is selected such that $W_1 = W_2 = 0.5$, $S = 0.5$, $E_1 = E_2 = 1$, $h_1 = h_2 = 0.5$, $h_0 = 1$, $F_1 = F_2 = 1$, $NW1 = 7$ with the strips up then down. The two dielectric constants of the substrates, ε_{r1} and ε_{r2}, were then both set equal and varied from 1 to 20. The same geometry was then tested with the microstrip above a ground plane as shown in Fig. 1, (open structure). Figures 10 and 11 show the coupling coefficient and the normalized phase velocity as a function of ε_{r1} and ε_{r2}, respectively. As shown in Fig. 10, the coupling coefficient, k_e, decreases as the dielectric constant is increased. However, with the strips down, the coupling coefficient, k_e, increases as ε_{r1} and ε_{r2} increases. That could be simply explained by the fact that the upper substrate is actually behaving as an overlay when the strips are down. This behavior of the microstrip transmission line with an overlay on top of the strips is investigated in depth in [7,22]. Since the coupling capacitance between the two conductors is directly proportional to the dielectric material, the coupling coefficient is thus expected to increase as ε_{r1} increases. It should also be noted that the difference in the odd and even normalized phase velocities, ν_e and ν_o, shown in Fig. 11 (strips down) is approximately zero. For this specific geometry, the distortion on the transmission line is almost eliminated. The results shown in Figs. 10 and 11 also show the advantage of using an embedded microstrip compared to an open one. By using the embedded microstrip, the coupling between the strips is decreased by approximately 0.6 dB, as shown in Fig. 10 (strips up). Consequently, distortion on the line is reduced. This phenomenon is also clearly shown in Fig. 11 (strips up), where $\nu_e - \nu_o$ for the embedded lines is closer to the zero line compared to the case with a microstrip above a ground plane. Figure 12 shows the coupling (C_{12}) and self (C_{11}) capacitances as a function of the dielectric constant of the substrates, ε_{r1} and ε_{r2}. The linearity behavior of the capacitances as ε_{r1} and ε_{r2} increase is clearly depicted in the figure. This phenomenon, however, is restricted to having only one homogeneous medium.

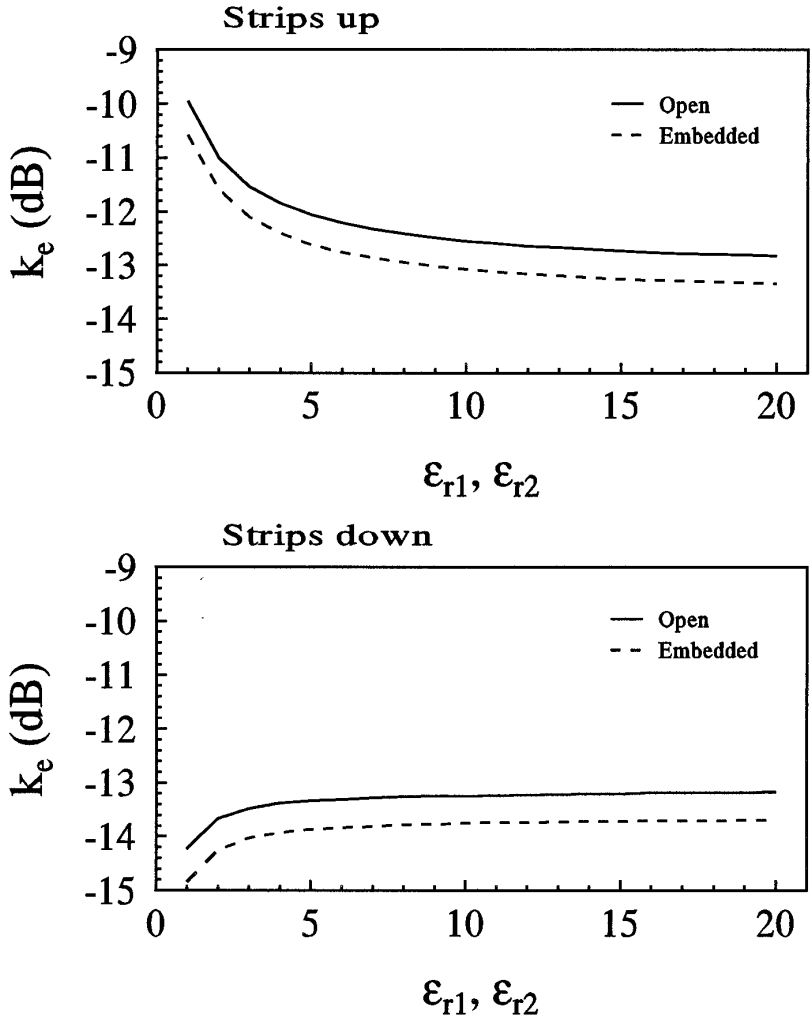

Figure 10. Coupling coefficient vs ε_{r1}, ε_{r2} ($W_1 = W_2 = 0.5$, $S = 0.5$, $A = 3.5$, $E_1 = E_2 = 1$, $h_1 = h_2 = 0.5$, $h_0 = 1$, $F_1 = F_2 = 1$, $NW1 = 6$).

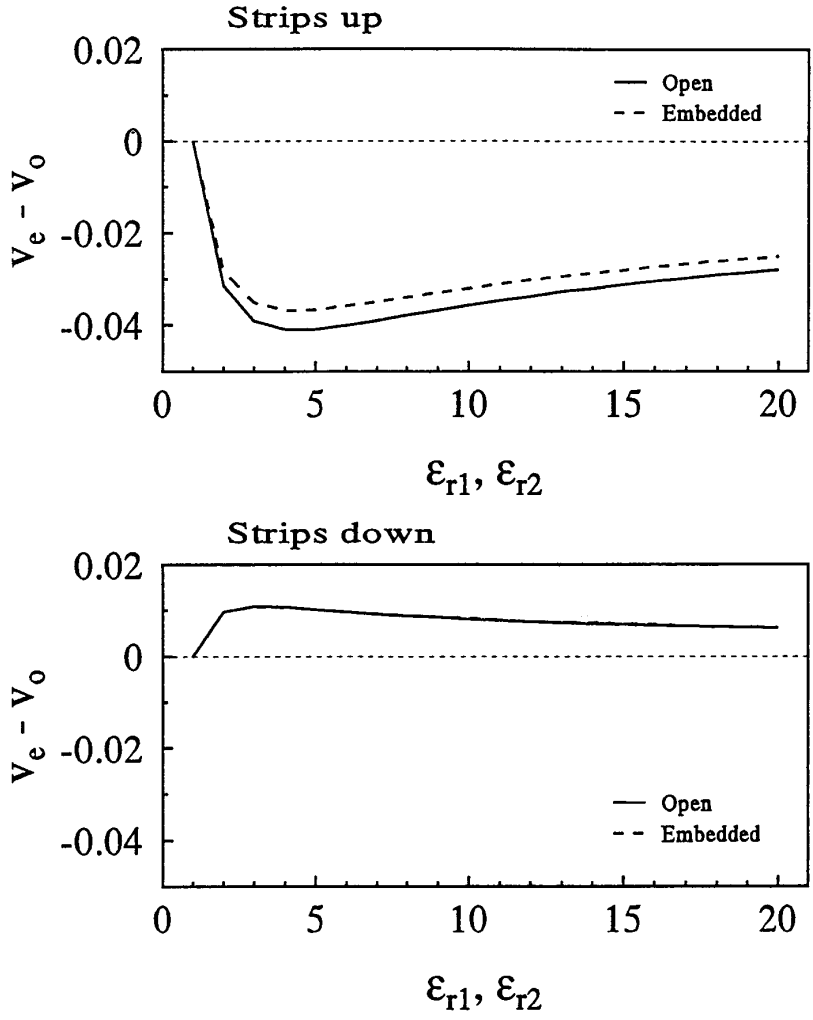

Figure 11. Difference in normalized phase velocity vs ε_{r1}, ε_{r2} ($W_1 = W_2 = 0.5$, $S = 0.5$, $A = 3.5$, $E_1 = E_2 = 1$, $h_1 = h_2 = 0.5$, $h_0 = 1$, $F_1 = F_2 = 1$, $NW1 = 6$).

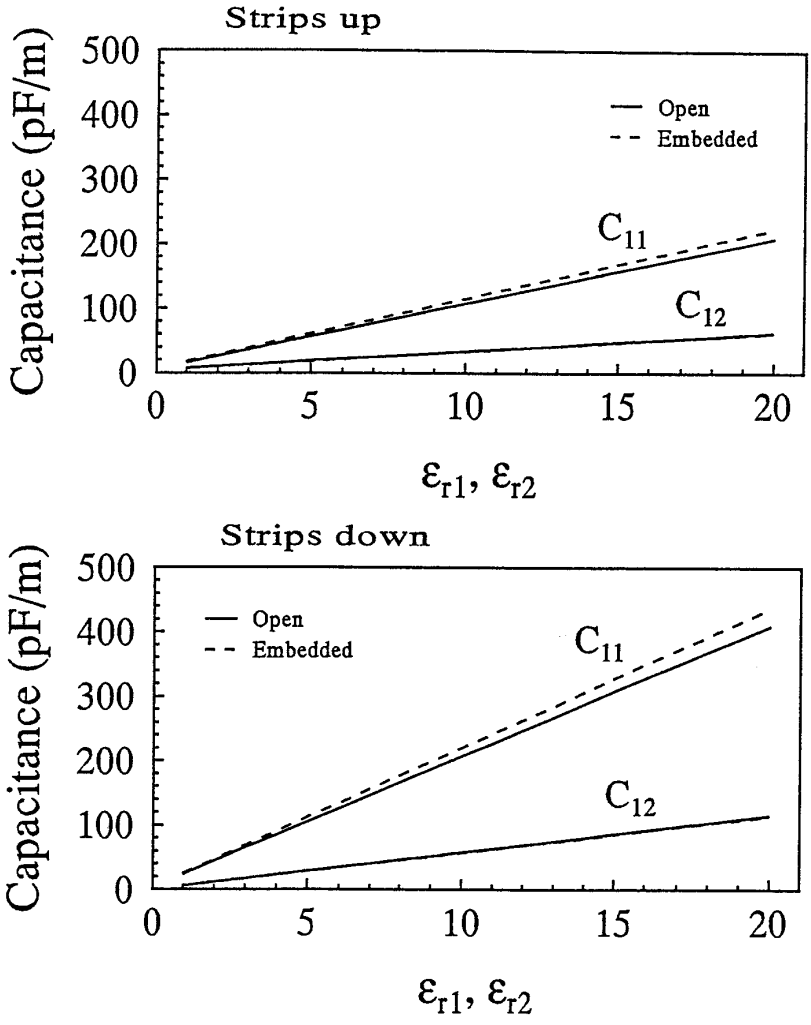

Figure 12. Self and mutual capacitance vs ε_{r1}, ε_{r2} ($W_1 = W_2 = 0.5$, $S = 0.5$, $A = 3.5$, $E_1 = E_2 = 1$, $h_1 = h_2 = 0.5$, $h_0 = 1$, $F_1 = F_2 = 1$, $NW1 = 6$).

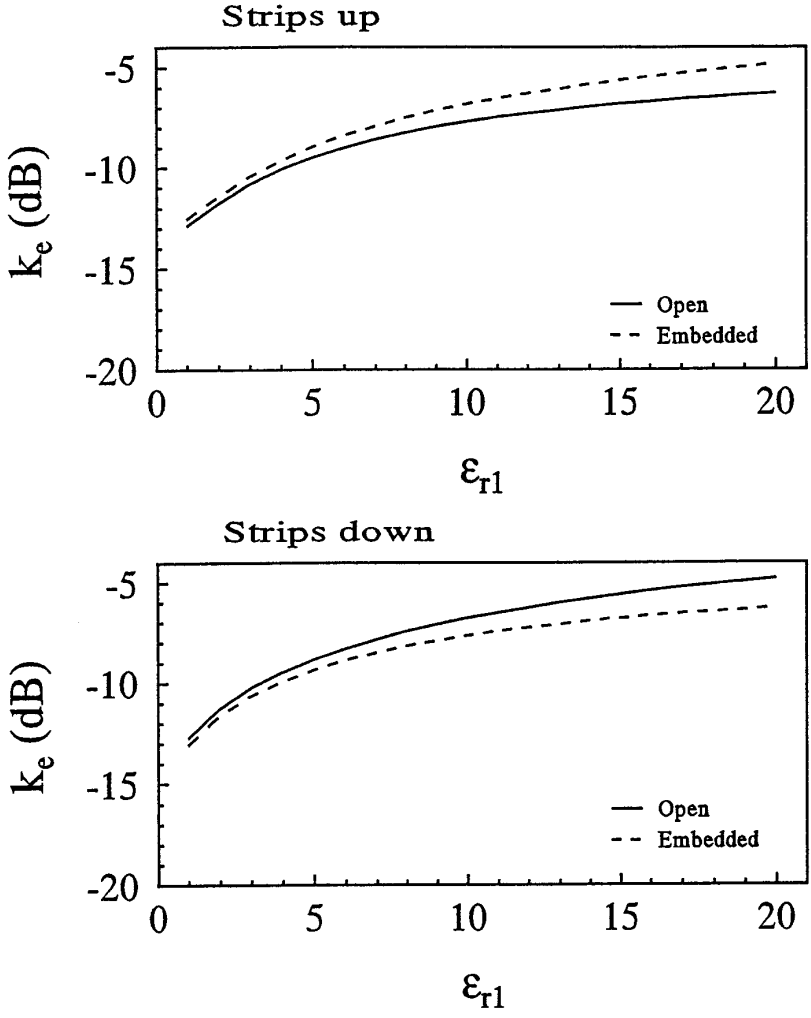

Figure 13. Coupling coefficient vs ε_{r1} ($W_1 = W_2 = 0.5,\ S = 0.5,\ A = 3.5,\ E_1 = E_2 = 1,\ h_1 = 0.2,\ h_2 = 0.8,\ h_0 = 1,\ F_1 = F_2 = 1,\ NW1 = 6$).

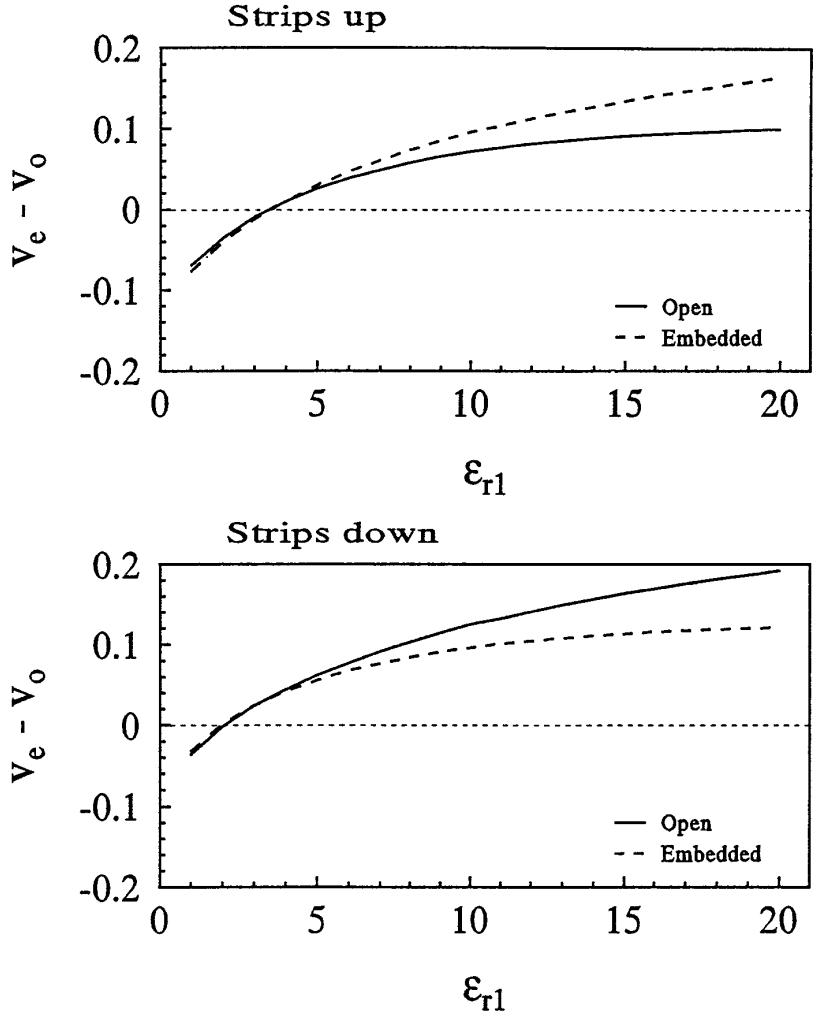

Figure 14. Difference in normalized phase velocity vs ε_{r1} ($W_1 = W_2 = 0.5, S = 0.5,\ A = 3.5,\ E_1 = E_2 = 1,\ h_1 = 0.2,\ h_2 = 0.8,\ h_0 = 1,\ F_1 = F_2 = 1,\ \varepsilon_{r2} = 2.2,\ NW1 = 7$).

Another geometry was picked to study the effect of the dielectric constant of the upper substrate, ε_{r1}, for the embedded and open MTLs. The geometry picked was such that $W_1 = W_2 = 0.5$, $S = 0.5$, $h_1 = 0.2$, $h_2 = 0.8$, $h_0 = 1$, $F_1 = F_2 = 1$, $\varepsilon_{r2} = 2.2$, and $NW1 = 7$. The dielectric constant of the upper substrate, ε_{r1}, was varied from 1 to 20. One notices that, for this case, the coupling coefficient increases as the dielectric constant of the upper substrate is increased, as shown in Fig. 13 (strips up). One also notices from Fig. 14 (strips up) that the ν_o and ν_e are equal at approximately $\varepsilon_{r1} = 3.5$. When the strips are down it has been found that the coupling coefficient increases as ε_{r1} increases, as shown in Fig. 13. However, in this case, ν_e and ν_o are equal for $\varepsilon_{r1} = 3.0$ as shown in Fig. 14. The same analysis, as in Figs. 13 and 14, was then repeated with $\varepsilon_{r2} = 9.7$. The behavior of the coupling and phase velocities is found to be basically the same as with $\varepsilon_{r2} = 2.2$. However, it is noticed that the coupling is significantly reduced compared to the case with $\varepsilon_{r2} = 2.2$. Also, the phase velocities are equalized at higher value of the dielectric constant of the upper substrate [20].

The effect of the separation distance between the two conductors was then studied. The geometry selected for that case was such that $W_1 = W_2 = 0.5$, $h_1 = 0.2$, $h_2 = 0.8, h_0 = 1$, $F_1 = F_2 = 1$, $\varepsilon_{r1} = 9.7$, $\varepsilon_{r2} = 2.2$, and $NW1 = 7$, with the strips up then down. The separation distance between the strips, S, was then varied from 0.1 to 2.2 while keeping the width of the MTL, A, equal to 3.5. From Fig. 15, it is clear that the coupling coefficient, k_e, decreases as the separation distance increases for both cases with strips up and down. Another important behavior of the microstrip is that at any separation between the strips, for the embedded microstrip case, it is possible to significantly reduce the coupling between the strips compared to the open microstrip structure. It is also worth noting that as the strips are separated, the odd and even mode characteristics of the line are also decoupled, as shown in Fig. 16, where the difference between ν_e and ν_o is almost zero. Another phenomenon that was also studied is the effect of varying the separation distance between the strips with a uniform dielectric medium. The same analysis was then repeated as in Figs. 15 and 16, however, in this case, the dielectric constants of the upper and lower substrates were both set equal to 9.7. It is very clear, from Fig. 17, that distortion is significantly reduced, compared to the case with two substrates. Also, with the strips down, it was possible to

equalize ν_e and ν_o at approximately S = 0.6. The dielectric constant of the substrates were then changed to $\varepsilon_{r1} = 2.2$ and $\varepsilon_{r2} = 9.7$. The coupling coefficient, is further reduced compared to that in Fig. 15, however, distortion is increased [20].

The height of the upper substrate is of great importance to the behavior of the microstrip transmission line, [23]. Usually, the height of the substrates should be selected carefully in order to equalize the phase velocities. To study the effect of this substrate height, a case was tested where $W_1 = W_2 = 0.5$, $S = 0.5$, $h_0 = 1$, $E_1 = E_2 = 1$, $F_1 = F_2 = 1$, $\varepsilon_{r1} = 9.7$, $\varepsilon_{r2} = 2.2$, and NW1 = 7 with the strips up then down. The height of the upper substrate, h_1, was then varied from 0.1 to 0.9. The coupling was reduced and showed a peak at $h_1 \cong 0.3$. When the strips are up, ν_e and ν_o are equal when the height of the substrate, h_1, is approximately 0.83 with the embedded MTL, and for the open MTL, ν_e and ν_o were equal at approximately $h_1 = 0.88$ [20]. The effect of varying the height of the upper substrate with the dielectric material of the upper and lower substrates equal to 2.2 and 9.7, respectively, was then investigated. For this case, the phase velocities did not intersect as shown in Fig. 18. It is clear, as shown in Fig. 19, that the coupling is reduced to almost -44 dB at h=0.9 compared to -16 dB with $\varepsilon_{r1} = 9.7$ and ε_{r2} =2.2. Hence, in order to reduce the coupling between the strips, the dielectric constant of the upper substrate should be smaller than that of the lower substrate. The same conclusion was also obtained in [24].

The effect of the width of the strips was then investigated. The geometry selected was such that $S = 0.5$, $h_1 = 0.2$, $h_2 = 0.8$, $h_0 = 1$, $E_1 = E_2 = 1$, $F_1 = F_2 = 1$, and $\varepsilon_{r1} = \varepsilon_{r2} = 9.7$, with the strips up then down. The width of the strips, W_1 and W_2, were then varied from 0.25 to 1.45. Figure 20 shows the coupling coefficient as a function of W_1 and W_2. It is clear that the strips get decoupled as their width increases. As shown in Fig. 21, for case with the strips down, and using the embedded microstrip line, it is possible to equalize the normalized phase velocities at $W_1 = W_2 = 1.35$. However, this was not possible with the open microstrip line. The same test was repeated with two different substrates, $\varepsilon_{r1} = 9.7$, ε_{r2} =2.2 or $\varepsilon_{r1} = 2.2$ and $\varepsilon_{r2} = 9.7$. It has been found that for this case, the normalized odd and even phase velocities are not equal anymore for any width of the strips [20].

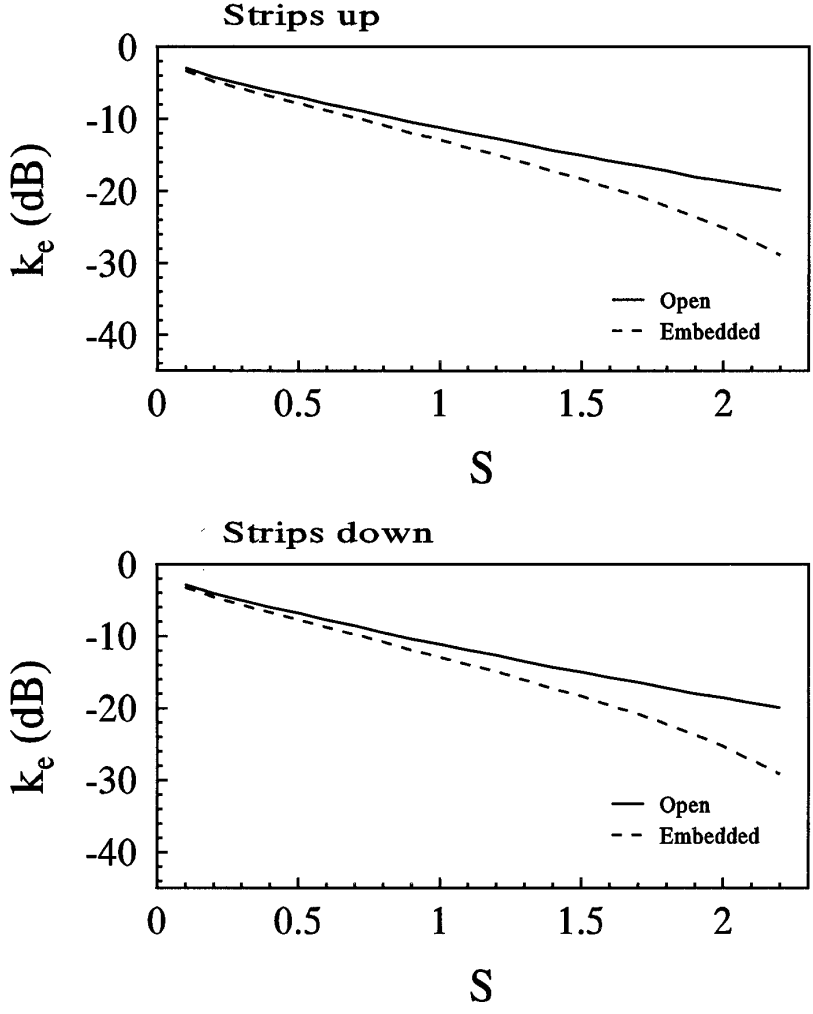

Figure 15. Coupling coefficient vs S ($W_1 = W_2 = 0.5,\ A = 3.5,\ h_1 = 0.2, h_2 = 0.8,\ h_0 = 1,\ F_1 = F_2 = 1,\ \varepsilon_{r1} = 9.7,\ \varepsilon_{r2} = 2.2,\ NW1 = 7$).

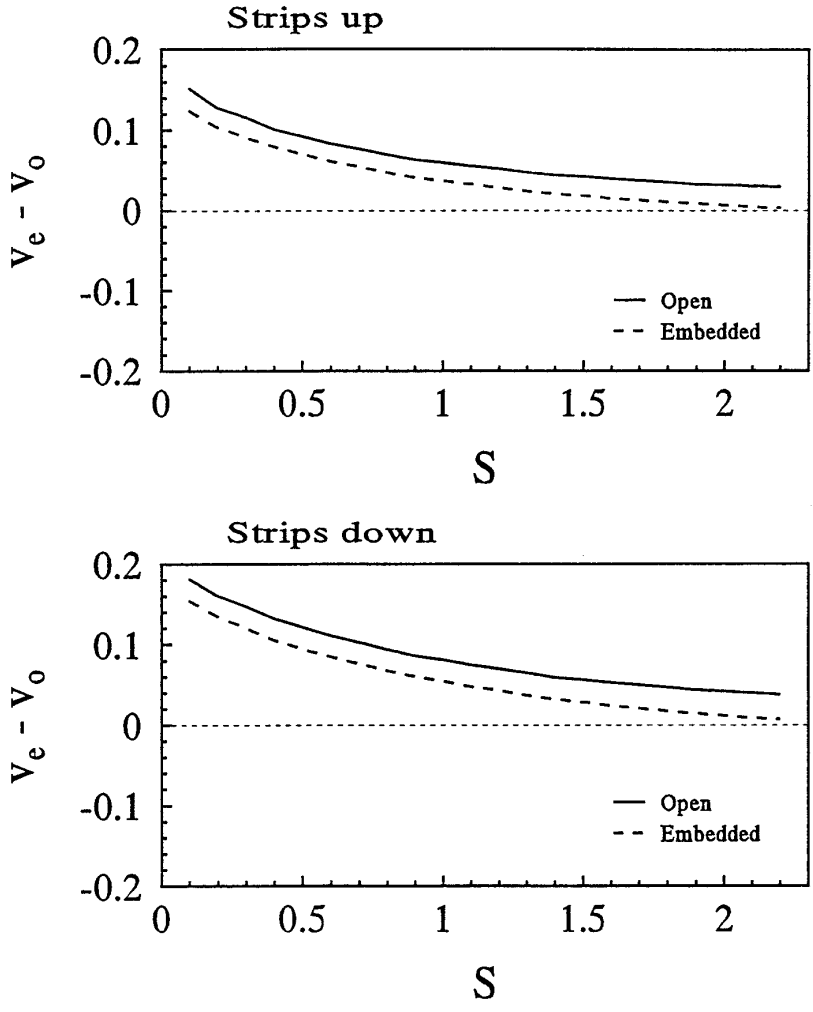

Figure 16. Difference in normalized phase velocity vs S ($W_1 = W_2 = 0.5$, $A = 3.5$, $h_1 = 0.2, h_2 = 0.8$, $h_0 = 1$, $F_1 = F_2 = 1$, $\varepsilon_{r1} = 9.7$, $\varepsilon_{r2} = 2.2$, $NW1 = 7$).

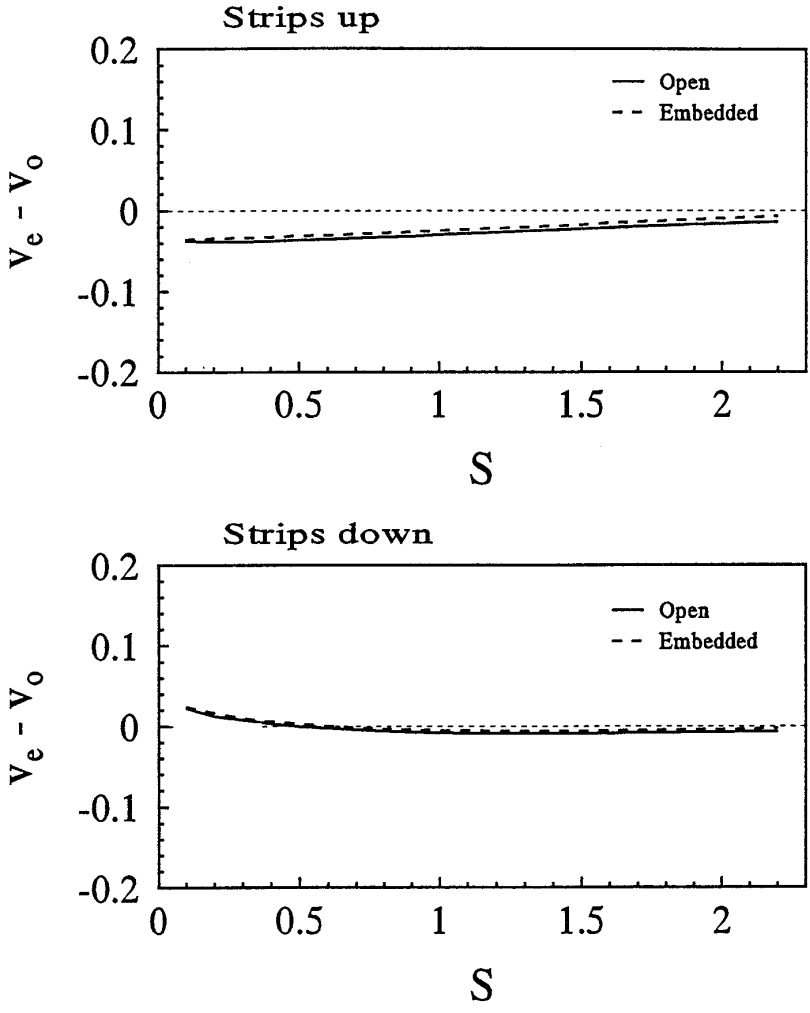

Figure 17. Difference in normalized phase velocity vs S ($W_1 = W_2 = 0.5$, $A = 3.5$, $h_1 = 0.2, h_2 = 0.8$, $h_0 = 1$, $F_1 = F_2 = 1$, $\varepsilon_{r1} = \varepsilon_{r2} = 9.7$, $NW1 = 7$).

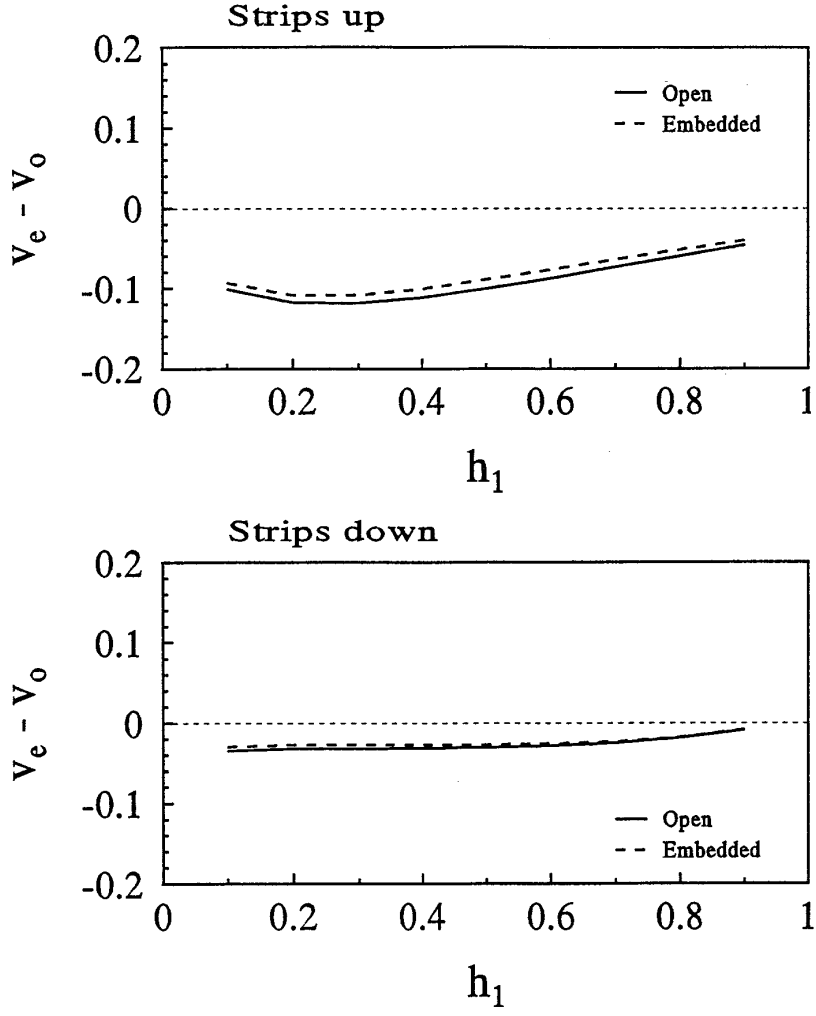

Figure 18. Difference in normalized phase velocity vs h_1 ($W_1 = W_2 = 0.5$, $S = 0.5$, $E_1 = E_2 = 1$, $h_0 = 1$, $F_1 = F_2 = 1$, $\varepsilon_{r1} = 2.2$, $\varepsilon_{r2} = 9.7$, $NW1 = 7$).

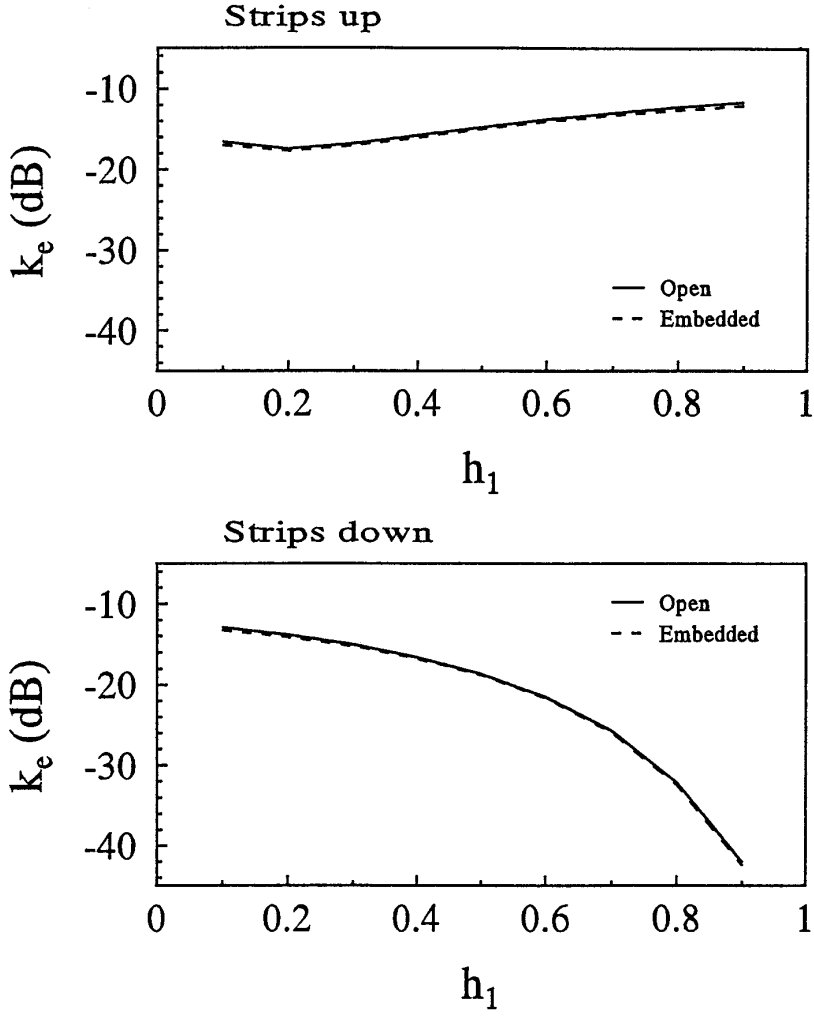

Figure 19. Coupling coefficient vs h_1 ($W_1 = W_2 = 0.5,\ S = 0.5,\ E_1 = E_2 = 1,\ A = 3.5,\ h_0 = 1,\ F_1 = F_2 = 1,\ \varepsilon_{r1} = 2.2,\ \varepsilon_{r2} = 9.7,\ NW1 = 7$).

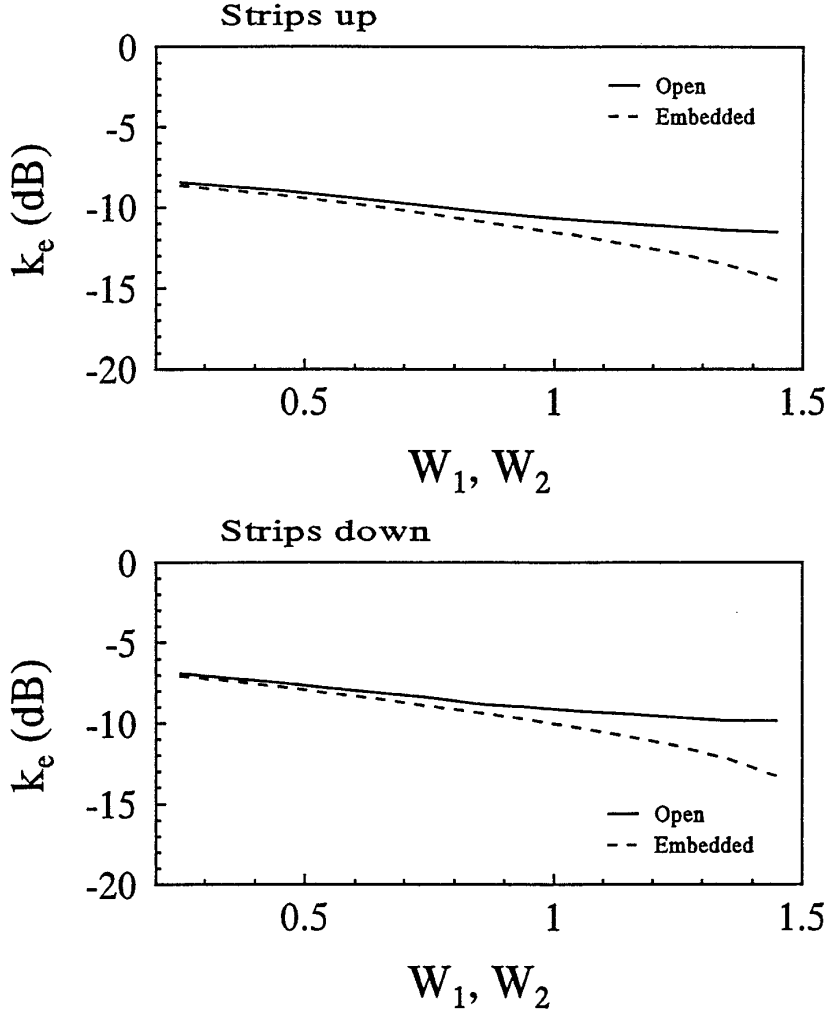

Figure 20. Coupling coefficient vs W_1, W_2 ($s = 0.25$, $h_1 = 0.2$, $h_2 = 0.9$, $h_0 = 0.2$, $F_1 = f_2 = 1$, $A = 3.5$, $\varepsilon_{r1} = 9.7$, $\varepsilon_{r2} = 9.7$).

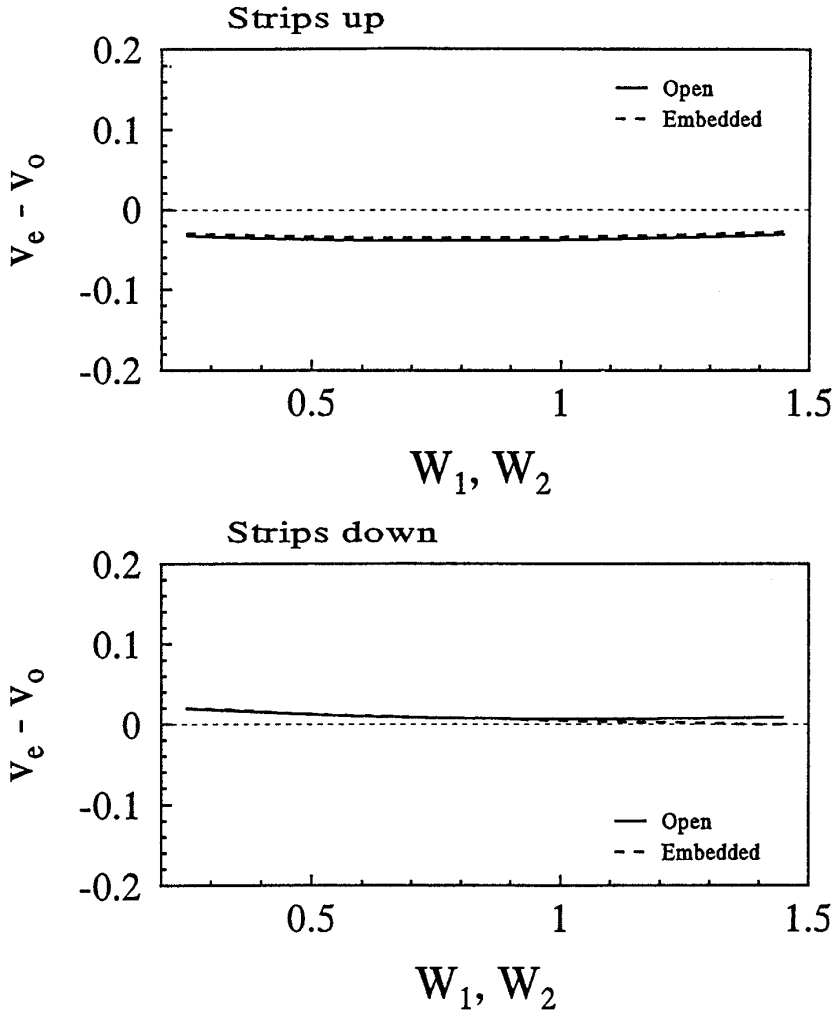

Figure 21. Difference in phase velocity vs W_1, W_2 ($s = 0.25$, $h_1 = 0.2$, $h_2 = 0.9$, $h_0 = 0.2$, $F_1 = f_2 = 1$, $A = 3.5$, $\varepsilon_{r1} = 9.7$, $\varepsilon_{r2} = 9.7$).

6. Summary and Conclusions

The finite difference technique has been used for the analysis of a two-conductor microstrip transmission line with two layers of dielectric substrate. The solution is based on a quasi-TEM approach where the thickness of the conductors is assumed to be zero. Dielectric materials are assumed to be lossless, isotropic, and homogeneous. Two different kinds of transmission lines have been investigated. The first is a microstrip transmission line located above a ground plane and the second is the same structure embedded in a ground plane. The procedure consists of formulating the necessary scalar potential equation at every node using second degree Lagrangian polynomials. Then, the total charge on the strip is computed using Gauss's law. Finally, from the total charge on the strips, the line capacitances, electrical coupling, odd and even phase velocities, and characteristic impedances of the transmission line are evaluated.

The coupling between circuit interconnection limits the bandwidth of dense microwave circuits and logic speed of digital and computing circuits and systems. Thus, it is usually desired to reduce the coupling on the lines. In this study, it is shown that the use of the embedded microstrip structure reduces the coupling between the strips and equalizes the phase velocities for a substrate of smaller dielectric constant compared to that needed for a microstrip above a ground plane. It is also shown that to significantly minimize the coupling, wider strips (smaller characteristic impedance) should be employed. In order to further reduce the coupling, it is suggested that the dielectric constant of the upper substrate be smaller than that of the lower one. It is also demonstrated that the self and mutual capacitances, for a homogeneous substrate, vary linearly as a function of the dielectric constant of the substrate. The results also indicated that the use of the embedded microstrip with two substrates can be used to reduce line coupling and to obtain distortionless transmission.

Acknowledgments

This work was supported in part by the U.S. Army Research Office under grant number DAAH04-94-G-0355. The authors would like to thank the reviewers for their constructive suggestions.

References

1. Weiss, J., "Microwave propagation an coupled Pairs of microstrip transmission Lines," *Advances in Microwaves,* New York, Academic Press, 295–320, 1974
2. Hamid, M., "A leaky stripline moisture sensor," *IEEE Trans. on Instrumentation and Measurement,* Vol. 41, No. 4, 550–562, August 1992.
3. Halim, M., and M. Hamid, "Fringing capacitance in thick-strip transmission line filters," *Electronic Letters,* Vol. 6, No. 9, April 1970.
4. Smith, C. E., "A coupled integral equation solution for microstrip transmission lines," *IEEE G-MTT Microwave Symp. Proc.,* 284–286, June, 1973.
5. Smith, C. E., and R. S. Chang, "Microstrip transmission line with finite-width dielectric," *IEEE Trans. Microwave Theory Tech.,* Vol. MTT-28, No. 2, 90–94, February 1980.
6. Smith, C. E., and R. S. Chang, "Microstrip transmission line with finite-width dielectric and ground plane," *IEEE Trans. Microwave Theory Tech.,* Vol. MTT-33, No. 9, 835–839, September 1985.
7. Elsherbeni, A. Z., C. E. Smith, B. Moumneh, H. Golestanian, and S. He, "Crosstalk reduction in integrated circuits and microwave/millimeter wave interconnections," *Final Report, the Army Research Office,* Technical Report No. 93-1, Department of Electrical Engineering, University of Mississippi, January 1993.
8. Yamashita, E., "Variational method for the analysis of microstrip-like transmission lines," *IEEE Trans. Microwave Theory Tech.,* Vol. MTT-16, No. 8, 529–535, August 1968.
9. Gladwell, G. M. L., "A Chebychev approximation method for microstrip problems," *IEEE Trans. Microwave Theory Tech.,* Vol. MTT-23, No. 11, 865–870, November 1975.
10. Cohn, S. B., "Shielded coupled-strip transmission line," *IRE Trans. Microwave Theory Tech.,* 29–38, October 1955.
11. Shimasaki, M., and T. Kiyono, "Analysis of microstrip transmission lines by an integral equations approach," *Electronics and Communications in Japan,* Vol. 54-B, No. 2, 80–88, 1971.
12. Kajfez, D., "Quasi-TEM modes on coupled transmission lines with asymmetric conductors," *Electrotechnical Review,* Vol. 44, No. 1, 1–9, 1977.

13. Kahaner, D., C. Moher, and N. Stephen, *Numerical Methods and Software,* New Jersey, Prentice Hall, 1989, Chapter 4.
14. Khebir, A., A. B. Kouki, and R. Mittra, "Absorbing boundary condition for quasi-TEM analysis of microwave transmission lines via the finite element method," *J. Electromagnetic Waves Appl.,* Vol. 4, No. 2, 145–157, 1990.
15. Gordon, R., and S. H. Fook, "A finite difference approach that employs an asymptotic boundary condition on a rectangular outer boundary for modeling two-dimensional transmission line structures," *IEEE Trans. Microwave Theory Tech.,* Vol. MTT-41, No. 8, 1280–1286, August 1993.
16. Kajfez, D., *Notes on Microwave Circuits,* Oxford, Mississippi, Kajfez Consulting, Vol. 2, Chapter 7, 1986.
17. Iskander, M. F., M. D. Morrison, W. C. Datwyler, and M. S. Hamilton, "A new course on computational methods in electromagnetics," *IEEE Trans. Education,* Vol. 31, No. 2, 101–115, May 1988.
18. Hoffmann, R. K., *Handbook of Microwave Integrated Circuits,* Norwood, Artech House, Chapter 9, 1987.
19. He, S., A. Z. Elsherbeni, and C. E. Smith, "Decoupling between two conductor microstrip transmission line," *IEEE Trans. Microwave Theory Tech.,* Vol. MTT-41, No. 1, 53–61, January 1993.
20. Elsherbeni, A. Z., B. Moumneh, and C. E. Smith, "Characteristics of two-conductor microstrip transmission lines embedded in a ground plane using the finite difference technique," *Technical Report,* No. 93-3, Department of Electrical Engineering, University of Mississippi, July 1993.
21. Pompei, D., O. Benevello, and E. Rivier, "Parallel line microstrip filters in an inhomogeneous medium," *IEEE Trans. Microwave Theory Tech.,* Vol. MTT-26, No. 4, 231–238, April 1978.
22. Elsherbeni, A. Z., C. E. Smith, H. Golestanian, and S. He, "Quasi characteristics of a two-conductor multilayer microstrip transmission line with dielectric overlay and a notch between the strips," *J. Electromagnetic Waves Appl.,* Vol. 7, No. 6, 769–789, 1993.
23. Gilb, J. K., and C. A. Balanis, "Pulse distortion on multilayer coupled microstrip lines," *IEEE Trans. Microwave Theory Tech.,* Vol. MTT-37, No. 10, 1620–1627, October 1989.

24. Elsherbeni, A. Z., B. Moumneh, C. E. Smith, and H. Golestanian, "Coupling between two-conductor muti-layer shielded microstrip transmission line," *Proc. of IEEE Southeastern Symposium on System Theory,* Tuscaloosa, AL, 6–10, March 1993.